# **Evolution of South Tropical Indian Ocean Warming and the Climatic Impacts Following Strong El Niño Events**

#### ZESHENG CHEN

State Key Laboratory of Tropical Oceanography, South China Sea Institute of Oceanology, Chinese Academy of Sciences, Guangzhou, China

### YAN DU

State Key Laboratory of Tropical Oceanography, South China Sea Institute of Oceanology, Chinese Academy of Sciences, Guangzhou, and University of Chinese Academy of Sciences, Beijing, China

#### ZHIPING WEN

Department of Atmospheric and Oceanic Sciences/Institute of Atmospheric Sciences, Fudan University, Shanghai, and Innovation Center for Climate Change, Nanjing, China

#### RENGUANG WU

Center for Monsoon System Research, Institute of Atmospheric Physics, Chinese Academy of Sciences, Beijing, China

#### SHANG-PING XIE

Scripps Institution of Oceanography, University of California, San Diego, La Jolla, California

(Manuscript received 22 October 2018, in final form 11 July 2019)

### **ABSTRACT**

The south tropical Indian Ocean (TIO) warms following a strong El Niño, affecting Indo-Pacific climate in early boreal summer. While much attention has been given to the southwest TIO where the mean thermocline is shallow, this study focuses on the subsequent warming in the southeast TIO, where the mean sea surface temperature (SST) is high and deep convection is strong in early summer. The southeast TIO warming induces an anomalous meridional circulation with descending (ascending) motion over the northeast (southeast) TIO. It further anchors a "C-shaped" surface wind anomaly pattern with easterlies (westerlies) in the northeast (southeast) TIO, causing a persistent northeast TIO warming via wind–evaporation–SST feedback. The southeast TIO warming lags the southwest TIO warming by about one season. Ocean wave dynamics play a key role in linking the southwest and southeast TIO warming. South of the equator, the El Niño–forced oceanic Rossby waves, which contribute to the southwest TIO warming, are reflected as eastward-propagating oceanic Kelvin waves along the equator on the western boundary. The Kelvin waves subsequently depress the thermocline and develop the southeast TIO warming.

### 1. Introduction

El Niño-Southern Oscillation (ENSO) is the strongest interannual variability in the tropics, affecting Indo-Pacific climate (e.g., Zhang et al. 1996, 1999; Wang et al. 2000; Chen 2002; Wu et al. 2003; Chen et al. 2017). In the positive phase of ENSO, El Niño forces the tropical

Corresponding author: Yan Du, duyan@scsio.ac.cn

Indian Ocean (TIO; 20°S–20°N) to warm up via surface heat flux change (Klein et al. 1999; Wu et al. 2008; Wu and Yeh 2010) and ocean dynamic processes (Xie et al. 2002; Liu and Alexander 2007; Du et al. 2009), like a battery charging a capacitor (Yang et al. 2007; Xie et al. 2009). When El Niño quickly decays and transits into a neutral or La Niña condition in the subsequent summer (here, the seasons refer to those for the Northern Hemisphere), the TIO warming persists through boreal

summer and unleashes its influence on Indo-Pacific climate (Xie et al. 2009, 2016). A tropospheric Kelvin wave-induced Ekman divergence mechanism (Xie et al. 2009) was proposed to explain the impact of TIO warming on the atmospheric circulation over the western North Pacific during boreal summer. In detail, the TIO warming forces a warm baroclinic Kelvin wave propagating eastward into the western Pacific. The surface divergence over the western North Pacific suppresses convection, in favor of the development or persistence of an anomalous anticyclone there. Such a salient anomalous anticyclone in lower troposphere over the western North Pacific plays an important role in modulating Indo-Pacific climate (e.g., Weisberg and Wang 1997; Wang et al. 1999; Wang et al. 2000; Chen 2002; Wang et al. 2003; Wu et al. 2010; Du et al. 2011; Zhan et al. 2011; Hu et al. 2011; Qu and Huang 2012; He et al. 2016; Chen et al. 2016).

In April–June (AMJ), most of the TIO belongs to part of the Indo-Pacific warm pool where the SST is above 28°C (Fig. 1a). Strong deep convection mainly occurs over the warm pool. The main rainbands are located over the eastern TIO, the intertropical convergence zone in Pacific, and the subtropical frontal region in East Asia (Fig. 1b). The mean zonal wind in the lower troposphere over the TIO is antisymmetric along the equator with easterly and westerly winds located south and north of the equator, respectively (Fig. 1c). During the El Niño decay phase, the south TIO warming plays a more active role in forcing the atmosphere (Du et al. 2009). The resultant antisymmetric wind anomaly pattern, which consists of anomalous easterly (westerly) winds in the north (south) TIO, contributes to the second peak warming in the north TIO in boreal summer (Du et al. 2009) via the wind-evaporation-SST feedback (Xie and Philander 1994; Xie 1996). The antisymmetric mode over the TIO during boreal spring (e.g., Wu et al. 2008; Du et al. 2009) may explain why the anomalies of low-level zonal wind, rainfall, and SST along the equator are weaker than those off the equator in AMJ (Figs. 1e,f,g).

In the southwest TIO (i.e., 12.5°–2.5°S, 50°–80°E; left red box in Fig. 1d) where the mean thermocline is shallow (e.g., Xie et al. 2002; Huang and Kinter 2002; Izumo et al. 2008; Du et al. 2009), both the surface heat flux change (Wu et al. 2008; Wu and Yeh 2010) and ocean wave dynamics contribute to the SST warming there. During El Niño, the negative wind stress curls in the central and eastern part of south TIO force downwelling oceanic Rossby waves slowly propagating westward. The oceanic Rossby waves deepen the thermocline and contribute to the SST warming in the southwest TIO (Xie et al. 2002). Such southwest

TIO warming may persist from boreal winter to early summer, and exert marked atmospheric influences as ENSO-related SST anomalies in the tropical Pacific decay quickly in boreal spring (Annamalai et al. 2005; Wu et al. 2008; Wu and Yeh 2010; Du et al. 2009; Xie et al. 2016).

The southeast TIO (i.e., 12.5°-2.5°S, 90°-112.5°E; right red box in Fig. 1d) is an important part of the Indo-Pacific warm pool during early summer (Fig. 1a) and supports strong deep convection (Fig. 1b). Although the SST variability is weaker in the southeast than southwest TIO (Fig. 1d), the rainfall variability in the southeast TIO is comparable to (or slightly stronger than) that in the southwest TIO (Fig. 1e). The SST anomalies in the southeast TIO can affect the Asian monsoon and climate in the adjacent regions (e.g., Wu et al. 2012; He and Wu 2014; W. Hu et al. 2014; Yang et al. 2015). Our study (i.e., Chen et al. 2018) also revealed that the southeast TIO warming during the decay phase of 2015/16 El Niño modulates the springtime and summertime lower troposphere circulation over the eastern TIO. It remains unclear whether these results are valid beyond this specific 2015/16 El Niño event.

The present study investigates the mechanism and impact of El Niño-induced surface warming over the south TIO, with a focus on the eastern subbasin. Specific science questions include the following: What is the respective effect of the southeast and southwest TIO warming on Indo-Pacific climate? What is the physical mechanism linking the warming in the east and west subbasins? While the El Niño-induced changes in shortwave radiation and surface latent heat flux are considered to be the main mechanism for the southeast TIO warming (e.g., Tokinaga and Tanimoto 2004; Wu et al. 2008; Chen et al. 2018), what is the role of ocean dynamics? Specifically, the El Niño-related surface wind stress curls over the southeast TIO force oceanic Rossby waves, which propagate westward. Even though the oceanic Rossby waves may dissipate during their westward journey, part of the energy could reach the African continent. Can they be reflected as eastward equatorial Kelvin waves and then influence the region off Sumatra in the eastern TIO? As the mean thermocline is deeper in the southeast than southwest TIO (Fig. 1b), the impact of the thermocline displacements on SST over the southeast TIO may not as effective as that over the southwest TIO. We show that such ocean wave processes may happen during a strong El Niño. This offers a physical explanation of why the southeast TIO warming always lags the southwest TIO warming by about one season. The southwest and southeast TIO warming in spring tends to work together inducing the north TIO warming in summer,

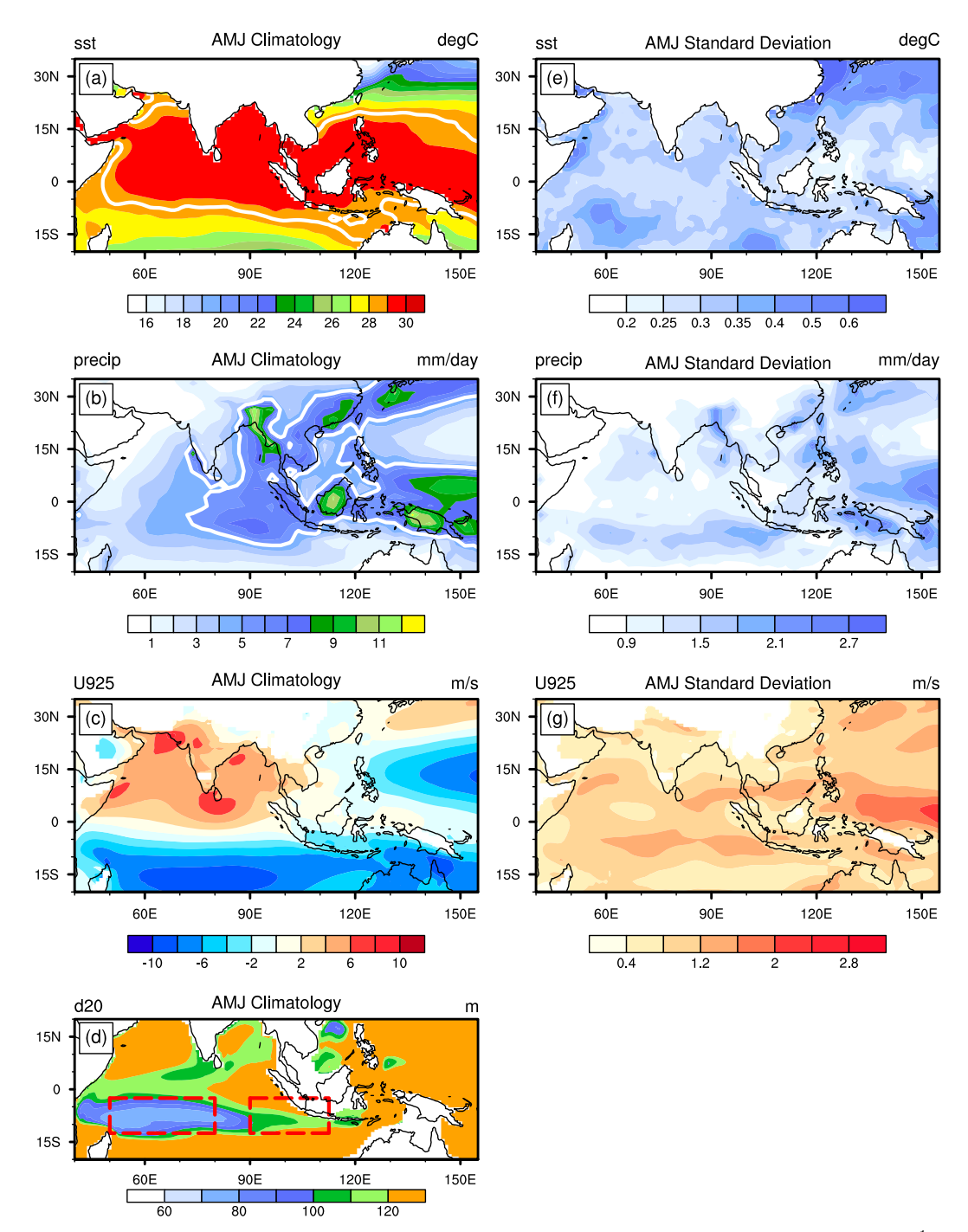


FIG. 1. Boreal late spring climatology for the period 1979–2016: (a) SST (°C), (b) GPCP precipitation (mm day $^{-1}$ ), (c) 925-hPa zonal wind (m s $^{-1}$ ), and (d) the thermocline depth (m). Also shown are late spring standard deviations for the same period for (e) SST (°C), (f) GPCP precipitation (mm day $^{-1}$ ), and (g) 925-hPa zonal wind (m s $^{-1}$ ). The white thick contours in (a) and (b) denote 28°C and 5 mm day $^{-1}$ , respectively. The southwest and southeast TIO are defined by the region encircled by the left (12.5°–2.5°S, 50°–80°E) and right (12.5°–2.5°S, 90°–112.5°E) box in (d), respectively.

thus modulating Indo-Pacific climate. Besides, the southeast TIO warming can directly affect East Asia-western North Pacific climate by inducing local anomalous meridional circulation. The rest of the manuscript is organized as follows. The datasets, methods, and atmosphere model used in this study are described in section 2. The specific reasons why we pay more attention to southeast TIO warming

during strong El Niño decaying years are provided in section 3. How southwest and southeast TIO warming modulate Indo-Pacific climate from El Niño decaying spring to early summer is illustrated in section 4. The connection between southeast and southwest TIO warming is shown in section 5. Finally, a summary and discussion are given in section 6.

### 2. Data and methodology

Precipitation data used in this study were from the Global Precipitation Climatology Project (GPCP; Adler et al. 2003). The GPCP monthly data on a 2.5° global grid were provided by the NOAA/OAR/ESRL PSD, Boulder, Colorado, and downloaded from their website at https://www.esrl.noaa.gov/psd/. Monthly SST data on a 1° × 1° grid were obtained from Met Office Hadley Centre Sea Ice and Sea Surface Temperature version 1.1 (HadISST1.1; Rayner et al. 2003). Atmospheric data were from European Centre for Medium-Range Weather Forecasts monthly mean reanalysis (ERA-Interim; Dee et al. 2011). The ERA-Interim dataset has a  $1^{\circ} \times 1^{\circ}$  horizontal resolution and extends from 1000 to 1 hPa with 37 vertical pressure levels. All above datasets are available from January 1979 to December 2016. In addition, the monthly mean sea surface heights from 1980 to 2016 were obtained from the National Centers for Environmental Prediction Global Ocean Data Assimilation System (GODAS; http://www.esrl.noaa.gov/ psd/data/gridded/data.godas.html). The daily mean sea surface heights from 1993 to 2016 with a  $0.25^{\circ} \times 025^{\circ}$ horizontal resolution from the Archiving, Validation, and Interpretation of Satellite Oceanographic Data (AVISO; http://marine.copernicus.eu/services-portfolio/access-toproducts/) are also used in this study. The seasonal anomalies were calculated by removing the climatological seasonal cycle and linear trend for the observations. Inclusion of linear trends does not change the main findings in this study (figures not shown). The confidence level of composite, correlation, and regression analysis is evaluated through two-tailed Student's t test.

As coherent signals can be seen in the East Asia-western North Pacific region in post-ENSO summer (e.g., Kosaka et al. 2013; K. Hu et al. 2014; Xie et al. 2016), we applied multivariate empirical orthogonal function (MV-EOF) analysis to extract the leading mode of East Asia-western North Pacific climate in May-July (MJJ) for the period 1979–2016. The MV-EOF analysis was applied to a set of meteorological fields (i.e., precipitation, 925-hPa zonal and meridional winds) in a domain of 5°–40°N and 95°–150°E. An MV-EOF analysis with a larger domain leads to similar results (figure not shown). Before the MV-EOF analysis,

TABLE 1. The list of ENSO decaying years when the absolute value of the D(-1)JF(0) Niño-3.4 SST index exceeds 0.5 standard deviations (positive for El Niño and negative for La Niña). Entries in boldface denote strong ENSO decaying years in which the absolute value of D(-1)JF(0) Niño-3.4 SST index is greater than 1.0 standard deviations. Here, the numerals "-1" and "0" signify the previous and current year, respectively.

El Niño decaying years	La Niña decaying years
1983, 1987, 1988, 1992, 1995, 1998, 2003, 2007, 2010, 2015, 2016	1984, <b>1985</b> , 1986, <b>1989</b> , 1996, <b>1999</b> , <b>2000</b> , 2001, 2006, <b>2008</b> , 2009, <b>2011</b> , 2012

all the input data were interpolated onto a  $2.5^{\circ} \times 2.5^{\circ}$  grid. To give each variable an equal weight, MJJ anomalies of each variable at each grid point were first normalized by their respective standard deviations, and then they were concatenated into an *N*-dimensional vector as the input vector for each year. The time length of all input vectors is 38, and *N* is the total number of the grid points for each variable in the selected domain. Finally, an area-weighted covariance matrix was constructed to perform MV-EOF analysis.

In general, ENSO is locked to boreal winter. Its relevant SST anomalies in the central to eastern Pacific increase in boreal summer, reach their peak in boreal winter, and quickly decay in ensuing boreal spring (e.g., Rasmusson and Carpenter 1982; Galanti and Tziperman 2000; Tziperman et al. 1997; An and Wang 2001). Thus, we used the December (-1)-January (0)-February(0) [D(-1)JF(0)] Niño-3.4 SST index to define an ENSO event. Here, the numerals "-1" and "0" denote the previous and current year, respectively. The Niño-3.4 SST index is calculated as the SST anomalies averaged in the Niño-3.4 region (i.e., 5°S-5°N, 170°-120°W). Table 1 lists the ENSO years defined in this study. We defined a year as a strong ENSO year when the magnitude of the D(-1)JF(0) Niño-3.4 SST anomalies exceeds 1 standard deviation (positive for El Niño and negative for La Niña). A year with a magnitude of D(-1)JF(0) Niño-3.4 SST anomalies between 0.5 and 1 standard deviation is defined as a weak ENSO year.

The Community Atmosphere Model version 4 (CAM4), which is also the atmospheric component of Community Climate System Model version 4 (Gent et al. 2011), was used in this study. CAM4 was developed with significant community collaboration at the National Center for Atmospheric Research (Neale et al. 2013). In this study, the CAM4 model used finite-volume dynamical core (Lin 2004), and it was run at a horizontal resolution equivalent to  $0.9^{\circ} \times 1.25^{\circ}$ , with 26 vertical levels with a hybrid sigma-pressure coordinate system extending from the surface to about 3.5 hPa.

We conducted three sets of model experiments, including one control run (CTRL run) and two sensitivity runs (SETIO run and SWTIO run). The CTRL run is forced by climatological mean annual cycle of SSTs. The climatological SSTs in the CTRL run are derived from a merged SST product, which was specifically developed as boundary conditions for atmosphere general circulation model (Taylor et al. 2000; Hurrell et al. 2008). The SETIO (SWTIO) run is forced by SSTs, obtained by superimposing the idealized SST anomalies shown in Fig. 2 in the southeast (southwest) TIO onto the climatological mean annual cycle of SST in the global ocean. The idealized SST anomalies are constructed by formula:  $0.8 \exp(-\{a[(x-b)/360]\}^4) \exp\{-[(y+6.5)/90]^4\},$  where a = 35 (30) and b = 100 (65) for the SETIO (SWTIO) run. The center of SST anomalies in the SETIO (SWTIO) run is located at  $-6.5^{\circ}$ S ( $-6.5^{\circ}$ S) and  $100^{\circ}$ E (65°E) with the maximum SST anomaly reaching 0.8°C. The area mean SST anomaly in the southeast TIO is about 0.403°C, and the counterpart in the southwest TIO is 0.395°C. Each run is a 35-yr continuous simulation, and the ensemble mean of last 30 years' results is analyzed in this study. A two tailed Student's t test is utilized to evaluate the confidence level of the differences between sensitivity run and CTRL run.

# **3.** Two key regions in the south TIO during spring to summer transition

Figure 3a shows the dominant mode of East Asiawestern North Pacific climate during early summer (MJJ). Spatially coherent anomaly pattern between precipitation and wind in the lower troposphere is revealed by the MV-EOF1. The MV-EOF1 accounts for 22.6% of the total variance of all three fields, and its eigenvalue is significantly separated from others according to the method of North et al. (1982). The positive values of principal component are associated with an anomalous anticyclone, with southwesterly wind anomalies prevailing over the northern South China Sea through the middle and lower reaches of the Yangtze River and easterly wind anomalies lying between 5° and 20°N. An elongated positive rainfall anomaly band appears along the Yangtze River Valley to southern Japan, whereas the Indochina Peninsula, the South China Sea, and the Philippine Sea receive less rainfall (Fig. 3a). The time series of MV-EOF1 visually features interannual variations (Fig. 3b), and it is highly correlated with the D(-1)JF(0) Niño 3.4 SST index with a correlation coefficient of about 0.76. This implies that such a climatic mode over the East Asia-western North Pacific region in early summer is significantly associated with ENSO in the previous winter. Table 2 lists the strong positive and

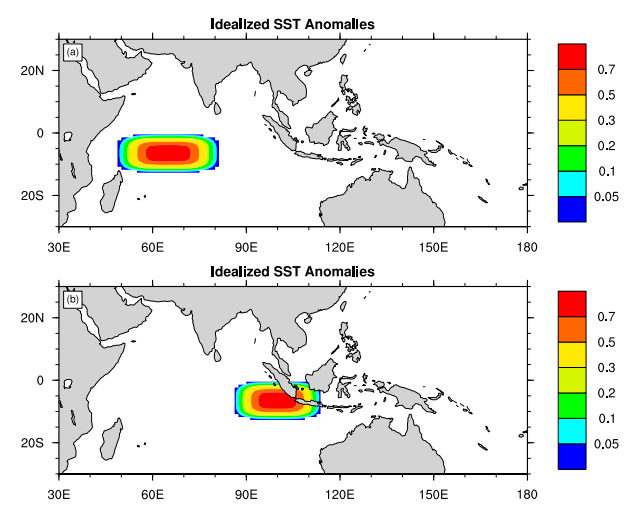


FIG. 2. Time-invariant SST anomalies from February to September used to drive CAM4 sensitivity experiments.

negative years of the MV-EOF1 principal component. Based on the 0.75 standard deviation criterion, 10 cases are selected for both the positive and negative years of the MV-EOF1, and 70% (i.e., 7 out of 10) of the positive (negative) cases are preceded by El Niño (La Niña) in previous winter. Note that 5 (3) out of 7 these El Niño (La Niña) years are strong El Niño (La Niña) years. If a stricter criterion (i.e., 1.0 standard deviation) is adopted, there are 6 (3) of 8 (5) strong positive (negative) cases corresponding to El Niño (La Niña) years, and 4 (0) out of 6 (3) these El Niño (La Niña) years are strong El Niño (La Niña) years. Such results indicate that ENSO exerts its delayed influence on East Asia-western North Pacific climate during early summer (e.g., Wang et al. 2004; Yuan et al. 2008; Moron et al. 2009; Nguyen-Le et al. 2015), especially for strong El Niño cases.

Besides, the MV-EOF1 is significantly correlated with the SST variations in Indo-Pacific region during early summer (Figs. 3c,d). For example, the anomalous anticyclonic wind anomaly over the western North Pacific and South China is significantly related to the Indian Ocean basinwide warming and local western North Pacific cooling (east of the Philippines). Enhanced convection is observed over the southeast TIO, the western part of Maritime Continent and the southwest TIO (Fig. 3d). Suppressed convection is found over the western North Pacific. In addition, an antisymmetric wind anomaly pattern is clear over the TIO with anomalous easterly wind in the north and anomalous westerly wind in the south (Fig. 3d). Similar and even stronger signals can be found in AMJ (Fig. 3c).

Previous studies have explored the effect of SST variability over the western North Pacific and the TIO during boreal spring and summer, especially during

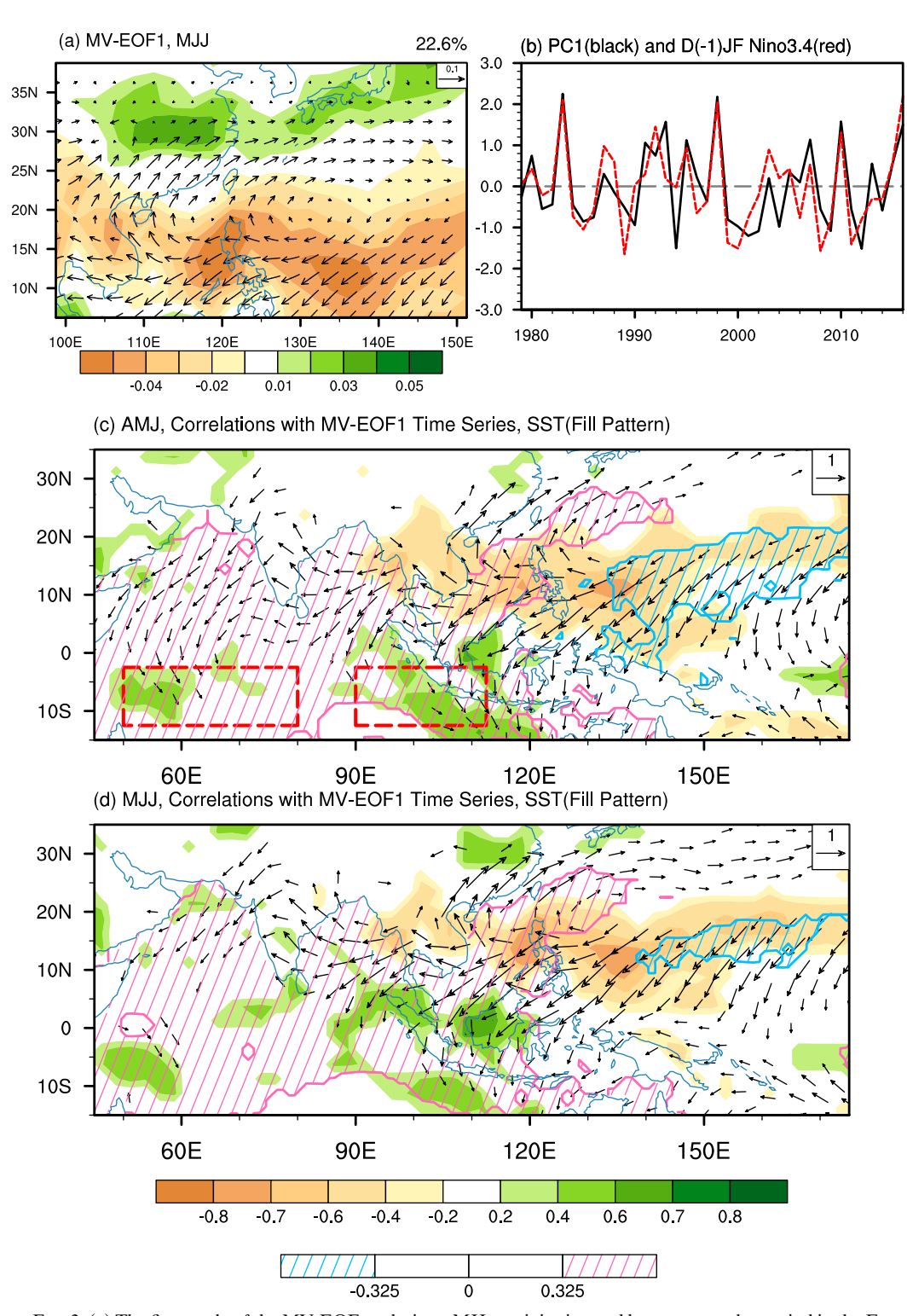


FIG. 3. (a) The first mode of the MV-EOF analysis on MJJ precipitation and lower troposphere wind in the East Asia—western North Pacific region. (b) The principal component of MV-EOF1 from 1979 to 2016 (black solid line) and previous wintertime Niño-3.4 index (red dashed line). Correlations with MJJ MV-EOF1 time series: (c) AMJ rainfall (shading), lower troposphere wind (vectors), and SST (fill pattern). (d) As in (c), but for MJJ. The values are plotted only exceeding the 95% confidence level according to the two-tailed Student's t test. The southwest (southeast) TIO is defined by the region encircled by the left (right) box in (c).

TABLE 2. The list of years when the absolute value of the MV-EOF1 principal component is greater than 0.75 (or 1.0) standard deviations. Entries in boldface denote ENSO decaying years listed in Table 1.

	Positive years	Negative years
0.75 standard deviation	1980, <b>1983</b> , 1991, <b>1992</b> , 1993, <b>1995</b> , <b>1998</b> ,	<b>1985</b> , <b>1986</b> , 1994, <b>1999</b> , <b>2000</b> , <b>2001</b> , 2002
	2007, 2010, 2016	2004, <b>2009, 2012</b>
1.0 standard deviation	<b>1983</b> , 1991, 1993, <b>1995</b> , <b>1998</b> , <b>2007</b> , <b>2010</b> ,	1994, <b>2001</b> , 2002, <b>2009</b> , <b>2012</b>
	2016	

the ENSO decaying phase (e.g., Wang et al. 2000; Watanabe and Jin 2002; Kug et al. 2006; Xie et al. 2009; Chen et al. 2016, 2017; Wu et al. 2018). Former studies demonstrated that the southwest TIO warming anchors the antisymmetric wind anomaly pattern over the tropical TIO during boreal spring (e.g., Wu et al. 2008; Du et al. 2009). W. Hu et al. (2014) show that the SST anomalies over southeast TIO have an impact on South China Sea and western North Pacific rainfall during early summer. He et al. (2016) found that South China Sea summer rainfall has a positive relationship with summer south Indian Ocean SST. Here, we focus on SST variability in the south TIO as well as its western and eastern subbasins (Fig. 3c). It is shown that anomalous warming (cooling) in the southeast and southwest TIO is significantly

associated with above (below) normal in situ rainfall from spring to summer (Fig. 4). In contrast, the SSTrainfall correlation is weakly negative and not as coherent in spatial distribution over most of the Bay of Bengal and South China Sea from spring to summer (Fig. 4). This implies that SST anomalies in the southeast and southwest TIO force atmospheric convective variability while SST variability in the Bay of Bengal and South China Sea is likely a response to atmospheric change from boreal spring to early summer (Zhou et al. 2018). Our results agree with Wu and Hu (2015), who also found a positive precipitation-SST correlation over the south TIO and weak negative simultaneous precipitation-SST correlation over the Arabian Sea and the Bay of Bengal during AMJ.

## SST and Precipitation Relationship

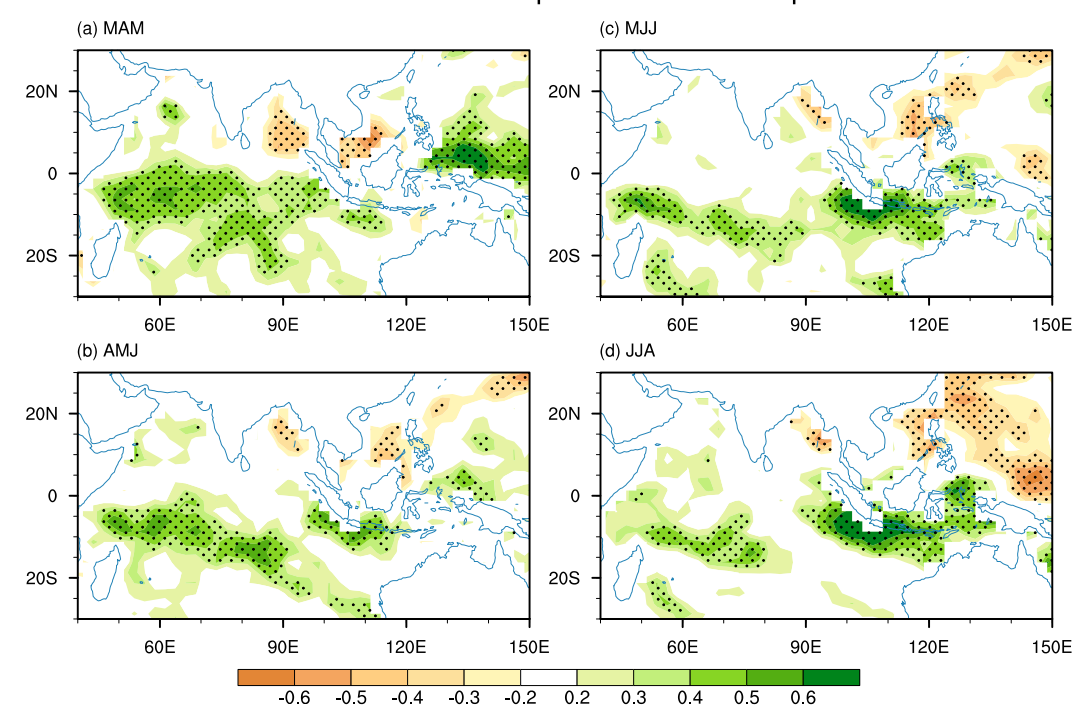


FIG. 4. Local point-to-point correlation between SST and precipitation. The stippling indicates 95% confidence levels based on the two-tailed Student's t test. Before calculating the relationship between SST and precipitation, the SST data on a  $1^{\circ} \times 1^{\circ}$  grid were interpolated into a  $2.5^{\circ} \times 2.5^{\circ}$  grid; thus the SST and precipitation data have the same horizontal resolution.

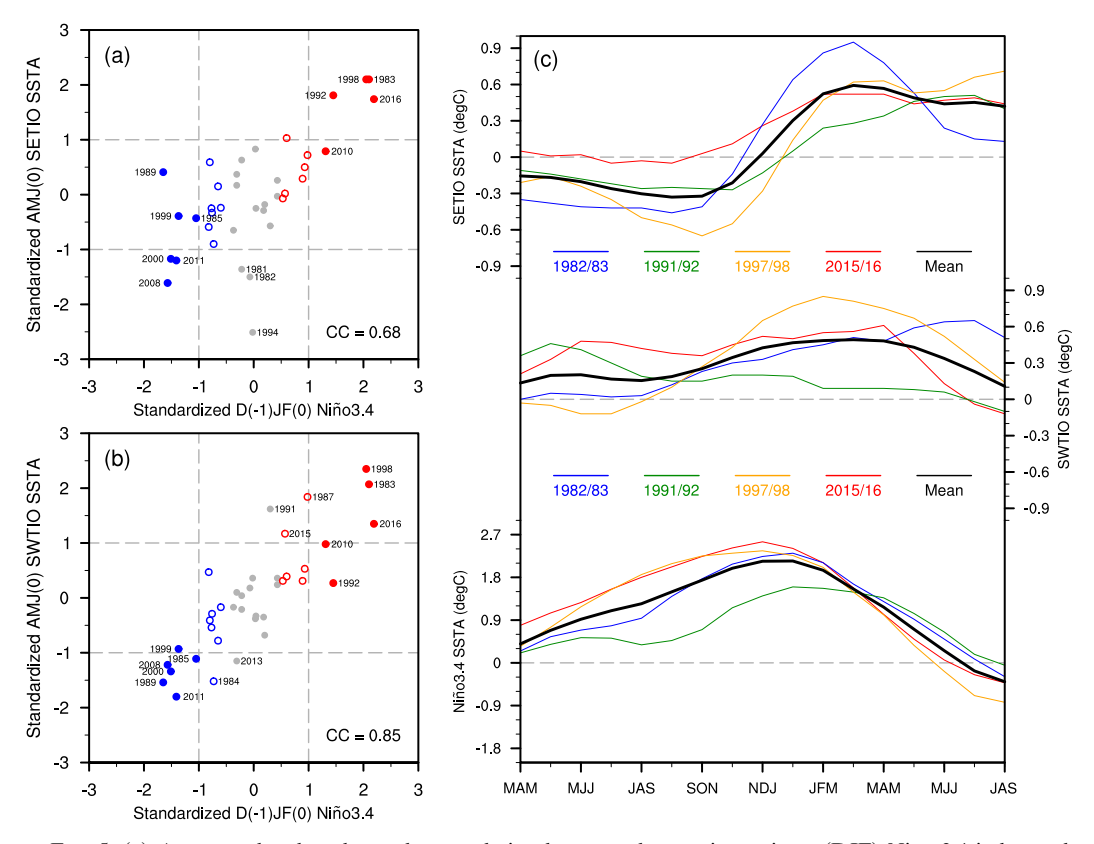


FIG. 5. (a) A scatterplot that shows the correlation between the previous winter (DJF) Niño-3.4 index and subsequent April–June (AMJ) SETIO SST index. (b) As in (a), but for SWTIO SST index. (c) The evolution of SST anomalies over the SETIO, SWTIO, and Niño-3.4 region from strong El Niño developing spring to decaying summer, respectively. CC is correlation coefficient; D(-1)JF(0) indicates December D(-1)JF(0) and similarly, AMJ(0) stands for April D(-1)JF(0) where numerals D(-1)JF(0) and current year, respectively. We marked the years in which the SST anomalies in the southeast (southwest) TIO are strong during boreal spring. Strong ENSO decaying years are also marked in the plot.

We computed the SST anomalies averaged in the southwest TIO (left box in Fig. 3c) and southeast TIO (right box in Fig. 3c) and refer to them as the SWTIO SST index and SETIO SST index, respectively. The correlation coefficient between the D(-1)JF(0) Niño-3.4 SST index and the AMJ(0) SWTIO (SETIO) SST index is around 0.85 (0.68). The responses of SST anomalies in the southwest TIO to ENSO seem to be more symmetric than those in the southeast TIO (Fig. 5b). Thus the southwest TIO SST anomalies have a closer relationship with ENSO (e.g., Xie et al. 2002; Izumo et al. 2008; Du et al. 2009).

Interestingly, 4 (3) out of 5 (6) strong southeast TIO warming (cooling) events are preceded by strong El Niño (La Niña) events in the previous winter (Fig. 5a), and in 4 (3) out of 5 (6) strong El Niño (La Niña) decaying years, strong southeast TIO warming (cooling) occurs in early summer (Fig. 5a). These results suggest that strong southeast TIO SST warming during late spring or early summer mainly appears in strong El Niño

ensuing years. Note that strong southeast TIO cooling is not always associated with strong La Niña decaying years (Fig. 5a). Such results reconfirm that the influence of La Niña on Indo-Pacific climate is not just a simple mirror image of El Niño (Okumura and Deser 2010; Chen et al. 2017). In the case that the southeast TIO SST anomalies feed back to the Indo-Pacific climate in early summer, the asymmetric performance of southeast TIO SST during ENSO decaying phase may partly explain why strong El Niño tends to exert stronger impact on Indo-Pacific climate during boreal early summer than strong La Niña does (Fig. 2b).

In the next section, we will consider the cases associated with previous strong El Niño condition and anomalous strong southeast TIO warming (i.e., years 1983, 1992, 1998, and 2016). In those cases, both southwest and southeast TIO warming can persist from boreal spring to summer (Fig. 5c). We will explore their possible role in modulating the East Asia—western Pacific climate from spring to early summer, respectively.

## Rainfall, SST and 925hPa Wind Anomalies

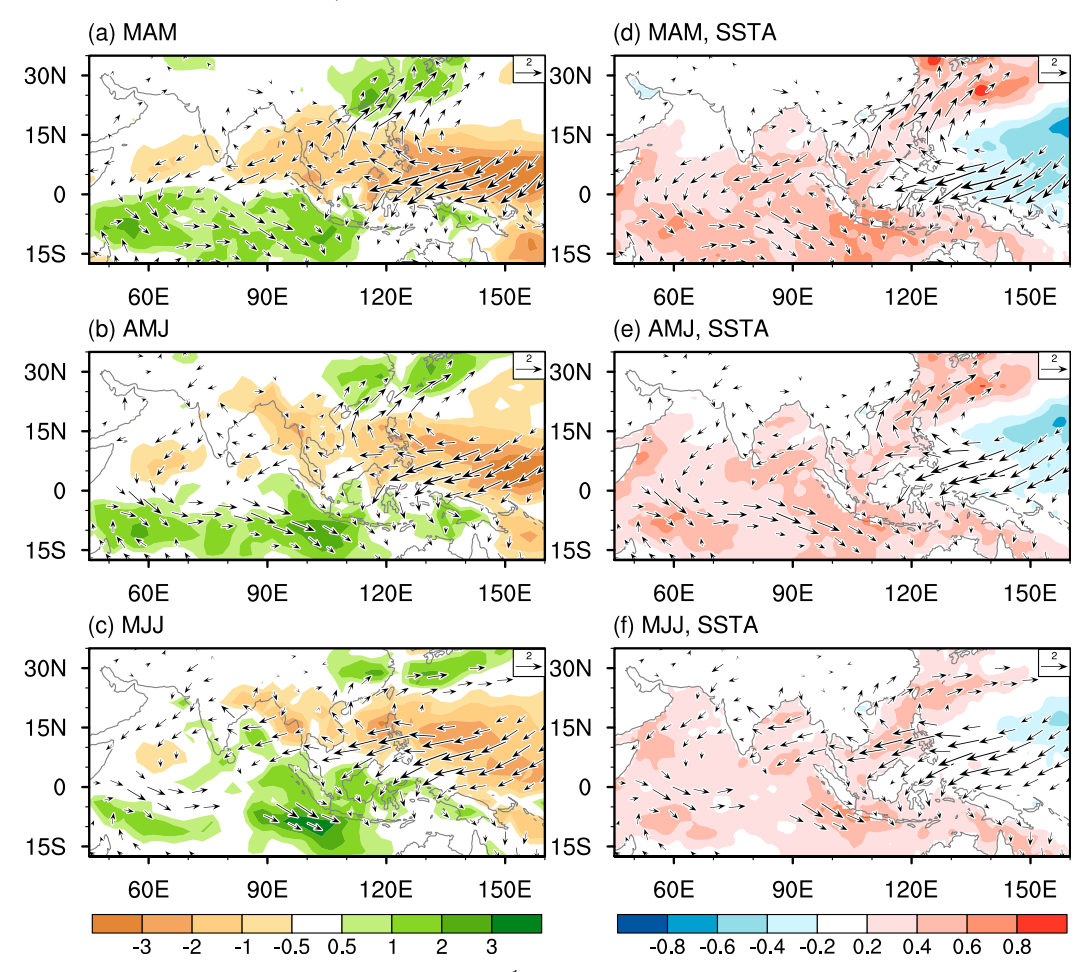


FIG. 6. The composites of (left) rainfall (mm day<sup>-1</sup>; shading) and (right) SST (°C; shading) and low-level wind (vectors) anomalies from strong El Niño decaying spring to early summer. Only the SST (rainfall and 925-hPa wind) anomalies that are significant at the 95% (90%) confidence level according to Student's t test are plotted.

# 4. Roles of southwest and southeast TIO warming in modulating Indo-Pacific climate

Figure 6 show the composited precipitation, SST, and low-level wind anomalies during strong El Niño decaying spring to early summer. In spite of TIO SST warming (Fig. 6d), the convection over the TIO is not enhanced in both the south and north Indian Ocean (Fig. 6). Instead, the precipitation anomalies over the TIO in boreal spring feature an antisymmetric pattern with more rainfall in the south and less rainfall in the north TIO, respectively (Fig. 6a). Such results are consistent with former studies (e.g., Wu et al. 2008; Du et al. 2009). Corresponding to such rainfall anomaly pattern, there are northwesterly and northeasterly wind anomalies in the south and north TIO, respectively (Fig. 6a). From spring to early summer, such antisymmetric mode is

slightly weakened in the western TIO (Fig. 6). In early summer, the deep convection is mainly enhanced over the western part of the Maritime Continent and adjacent southeast TIO (Fig. 6c), coinciding with suppressed deep convection over the Indochina Peninsula and South China Sea. Meanwhile, the precipitation anomaly signal over the western TIO is relatively weak compared to that over the eastern TIO (Fig. 6c).

Even though the El Niño cases selected in this study have their respective SST anomaly evolutions in the tropical Pacific and Indian Ocean, the anomalies over the Indo-Pacific have some common features. For example, anomalous anticyclonic wind anomalies can be found in the western North Pacific during El Niño decaying spring to summer (Fig. 6). The southwesterly wind anomalies on the western flank of anomalous anticyclonic facilitate the transport of lower troposphere

## Regressions with Standardized SETIO SST Index

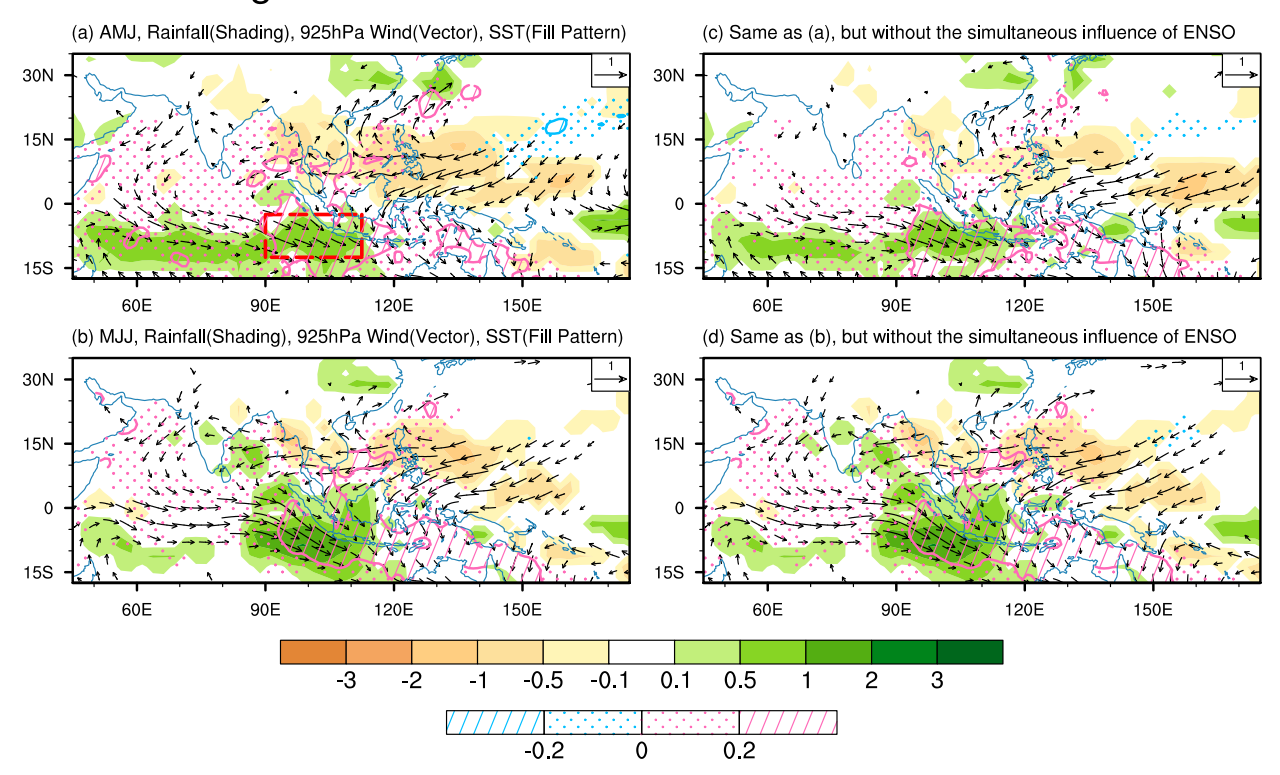


FIG. 7. Regression with the standardized SETIO SST index: precipitation (shading), low-level wind (vectors), and SST (fill pattern) for (a) AMJ and (b) MJJ with simultaneous ENSO influence, and for (c) AMJ and (d) MJJ without simultaneous influence of ENSO. Only the regressed anomalies that are significant at the 95% confidence level according to a two-tailed Student's *t* test are plotted. In (c) and (d), we computed the partial regression onto the SETIO SST index after excluding the regressed field onto the Niño-3.4 index in the simultaneous season.

water vapor from the tropical ocean region to subtropical areas (Wang et al. 2000). As a result, abovenormal rainfall extends from southeastern part of China to south of Japan (Fig. 6). Accordingly, there is asymmetric wind anomaly over the TIO with anomalous easterly wind in the north and anomalous westerly wind in the south (Fig. 6). Such asymmetric zonal wind anomaly pattern may be anchored by the south Indian Ocean warming that enhances deep convection in situ and triggers northerly wind anomalies across the equator (Fig. 6) (Wu et al. 2008). With the help of the Coriolis force off the equator, the northerly wind anomalies north (south) of the equator turn into northeasterly (northwesterly) wind anomalies. The asymmetric wind anomaly pattern over the TIO is robust in post-El Niño spring and summer. In early summer, it seems to split into two parts, one over the western TIO anchored by southwest TIO warming and the other over the eastern TIO anchored by southeast TIO warming (Fig. 6).

Over the southeast TIO, the maximum SST anomalies tend to lead the maximum rainfall anomalies by about 1 month (Fig. 11a). A similar relationship is also seen in

the southwest TIO (Fig. 11b). This suggests that the southeast and southwest TIO SST anomalies can modulate the adjacent or even remote atmosphere via inducing convective heating (e.g., Annamalai et al. 2005; W. Hu et al. 2014). The regression map with respect to the SWTIO or SETIO SST index indicates that both southwest and southeast TIO warming may exert impacts on the north Indian Ocean and South China Sea from spring to early summer (Figs. 7 and 8). The southeast TIO warming may have a more crucial impact on East Asia-western North Pacific rainfall in early summer (Figs. 7 and 8). However, during El Niño decaying phase, other factors, such as western North Pacific cooling (e.g., Wang et al. 2000) and central Pacific cooling (e.g., Chen et al. 2016), may also contribute to such wind anomalies over the western North Pacific. As the effects of those factors may co-occur with those of southeast and southwest TIO warming (Figs. 6–8), one may argue that we are likely to overstate the influence of southeast or southwest TIO SST anomalies on Indo-Pacific climate. It is really hard to extract the sole effect of southeast or southwest TIO warming from observations. The CAM4

## Regressions with Standardized SWTIO SST Index

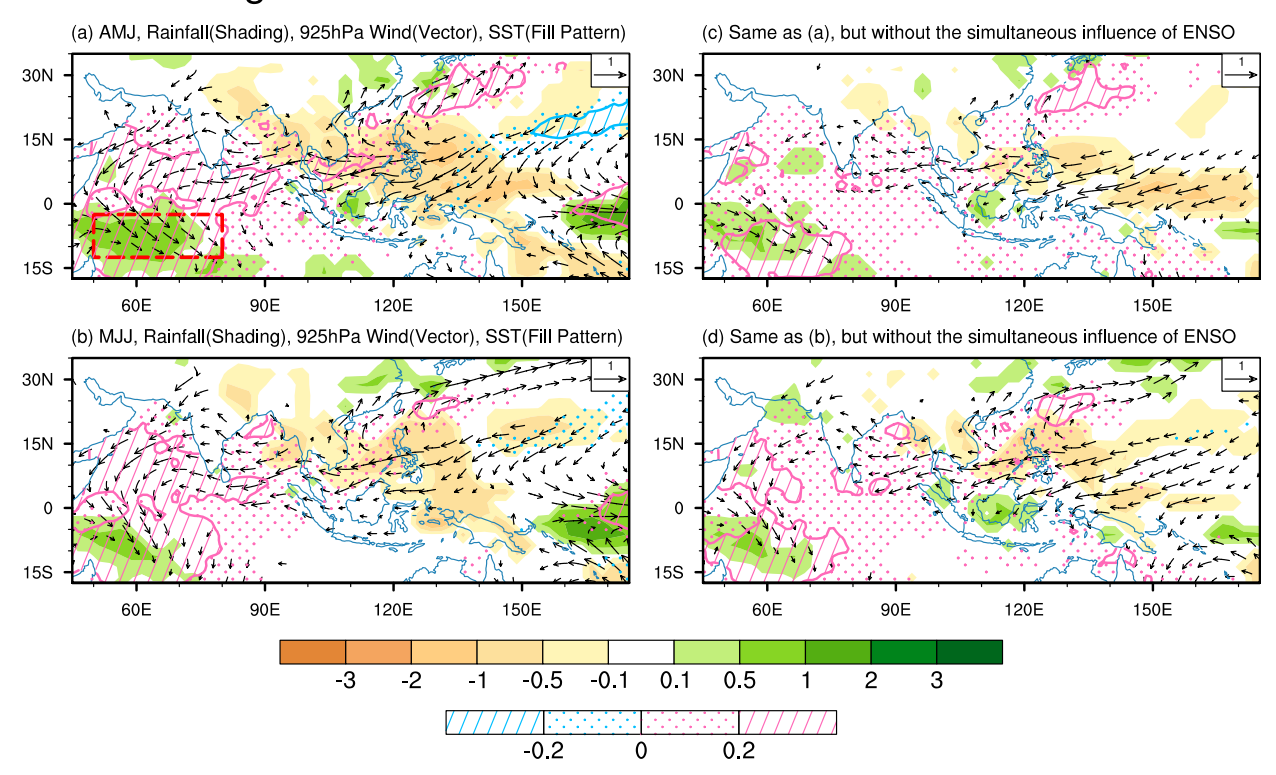


FIG. 8. As in Fig. 7, but for the results of the SWTIO SST index.

experiment forced with SST anomalies in specified ocean basin provides a useful illustration of regional SST effects. To further confirm the climatic impacts of southeast and southwest TIO SST warming, we designed a series of idealized CAM4 simulations (i.e., the CTRL run, SETIO run, and SWTIO run). The influence of the southeast (southwest) TIO SST warming is assessed by analyzing the ensemble mean differences between the SETIO (SWTIO) run and the CTRL run.

The CAM4 CTRL run can reasonably reproduce the major spatial features of the spring and summer climate in observation, such as the precipitation center over east TIO and western Pacific, the Somalia cross-equatorial jet, and westerly (easterly) winds blowing in the north (south) TIO in early summer (figure not shown). The spatial correlation coefficients between the simulated and observed climatological precipitation (zonal wind) fields in the region of 17.5°S-35°N, 45°-160°E for March-May (MAM), AMJ, and MJJ reach 0.81 (0.94), 070 (0.96), and 0.64 (0.97), respectively. Note that there are some deficiencies in the CTRL run. For example, the simulated subtropical rainband extending from South China to south Japan is weaker than observation, and the CTRL run overestimates (underestimates) the rainfall intensity in the north (equatorial) TIO (figure not shown).

Responses of precipitation and atmospheric circulation to southeast TIO warming are shown in Fig. 9. Clearly, the SETIO run well reproduces the observed asymmetric wind anomalies over the eastern TIO and anticyclonic wind anomalies over the western North Pacific (Fig. 6). Also, the meridional triple precipitation anomaly pattern, with more rainfall in the subtropical frontal region and southeast TIO and less rainfall in between, is reasonably captured by SETIO run (Fig. 6).

In response to the southeast TIO warming from spring to summer, the deep convection in situ is enhanced. Accordingly, the South China Sea, the Bay of Bengal, and the Philippines receive less rainfall, whereas the middle and lower reaches of the Yangtze River Valley receives more rainfall. The antisymmetric precipitation anomaly pattern over the east TIO is linked by a "C-shaped" wind anomaly pattern in lower troposphere. In spring, the C-shaped wind anomalies feature anomalous northeasterly (northwesterly) winds in the northern (southern) part of east TIO. These remain noticeable in boreal early summer (Fig. 9c).

Furthermore, there is a clear local meridional circulation from the eastern TIO to western tropical Pacific, as depicted by the upper-level velocity potential response. In response to southeast TIO warming, the

## The Differences between SETIO run and CTRL run

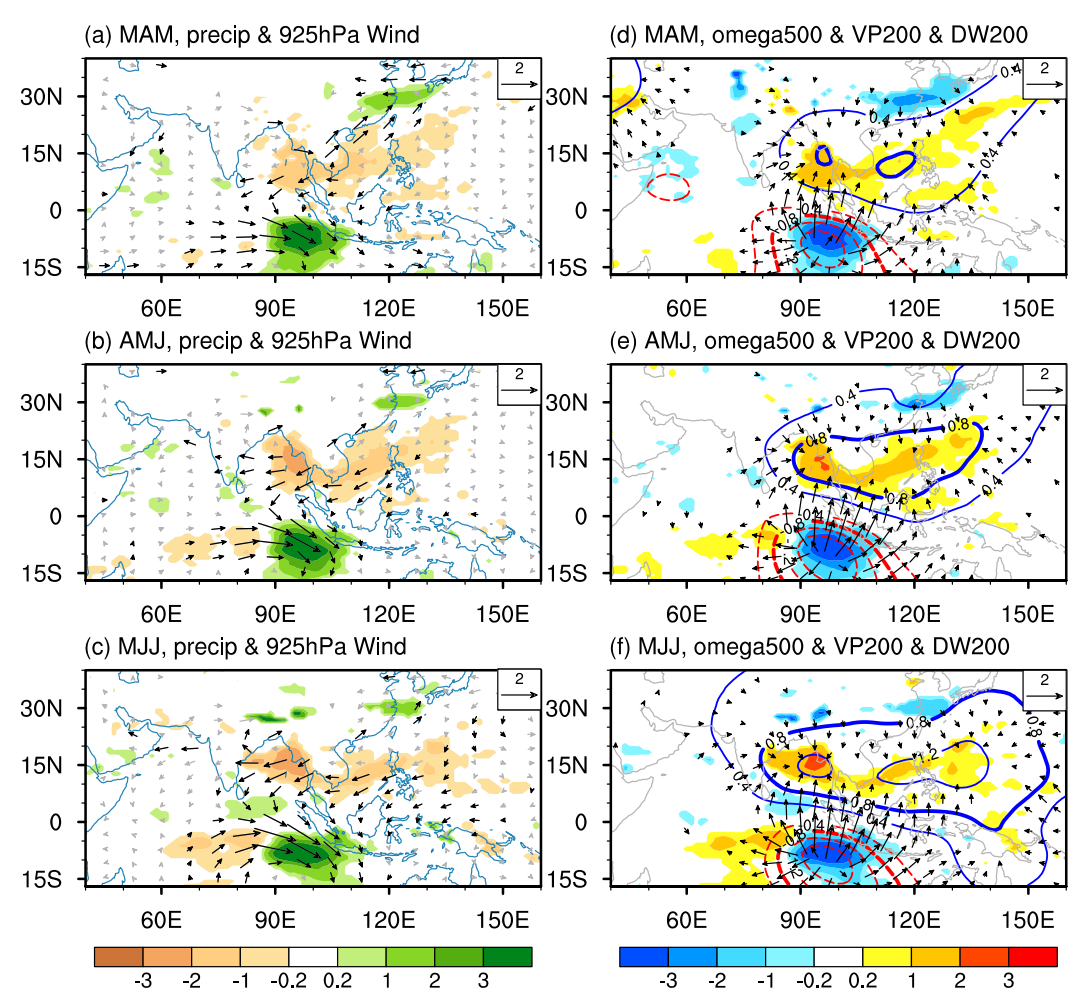


FIG. 9. The differences between the SETIO run and CTRL run: (a)–(c) precipitation (mm day<sup>-1</sup>; shading) and 925-hPa wind (m s<sup>-1</sup>; vectors) and (d)–(f) 500-hPa p velocity ( $10^{-2}$  Pa s<sup>-1</sup>; shading), 200-hPa velocity potential ( $10^6$  m<sup>2</sup> s<sup>-1</sup>; contours), and 200-hPa divergent wind (m s<sup>-1</sup>; vectors). The black vectors denote that the wind anomalies are significant at the 95% confidence level according to the two-tailed Student's t test. Only the precipitation and 500-hPa p velocity differences that are significant at the 95% confidence level are plotted.

200-hPa velocity potential response features a southnorth dipole pattern with a negative center over the
southeast TIO and a positive center over the Bay of
Bengal and South China Sea (Fig. 9). The updraft is
enhanced over the southeast TIO in relation to upperlevel (lower-level) divergence (convergence) in situ. At
the same time, upper-level (lower-level) convergence
(divergence) appears near the Bay of Bengal and South
China Sea, which is accompanied by anomalous downdraft there. Such local meridional circulation response
to southeast TIO warming directly connects the Bay of
Bengal and South China Sea climate to the southeast
TIO SST warming (Fig. 9). Besides, through modulating
the intensity of the anticyclonic circulation over the
South China Sea or the Asian summer monsoon, the

southeast TIO warming has an impact on eastern China rainfall (Fig. 9). The numerical results further confirm the possible influence of southeast TIO SST anomalies (e.g., Wu et al. 2012; Chen et al. 2014; He and Wu 2014; W. Hu et al. 2014) on Indo-Pacific climate from boreal spring to early summer.

The regression map with respect to the SETIO SST index also indicates that the southeast TIO warming contributes to the north TIO warming via air–sea coupling (Fig. 7). When monsoonal southwesterly winds prevail over the Bay of Bengal and South China Sea, the northeasterly wind response to southeast TIO warming facilitates the SST warming there via decreasing the wind speed and latent heat flux (Figs. 7 and 9).

## The Differences between SWTIO run and CTRL run

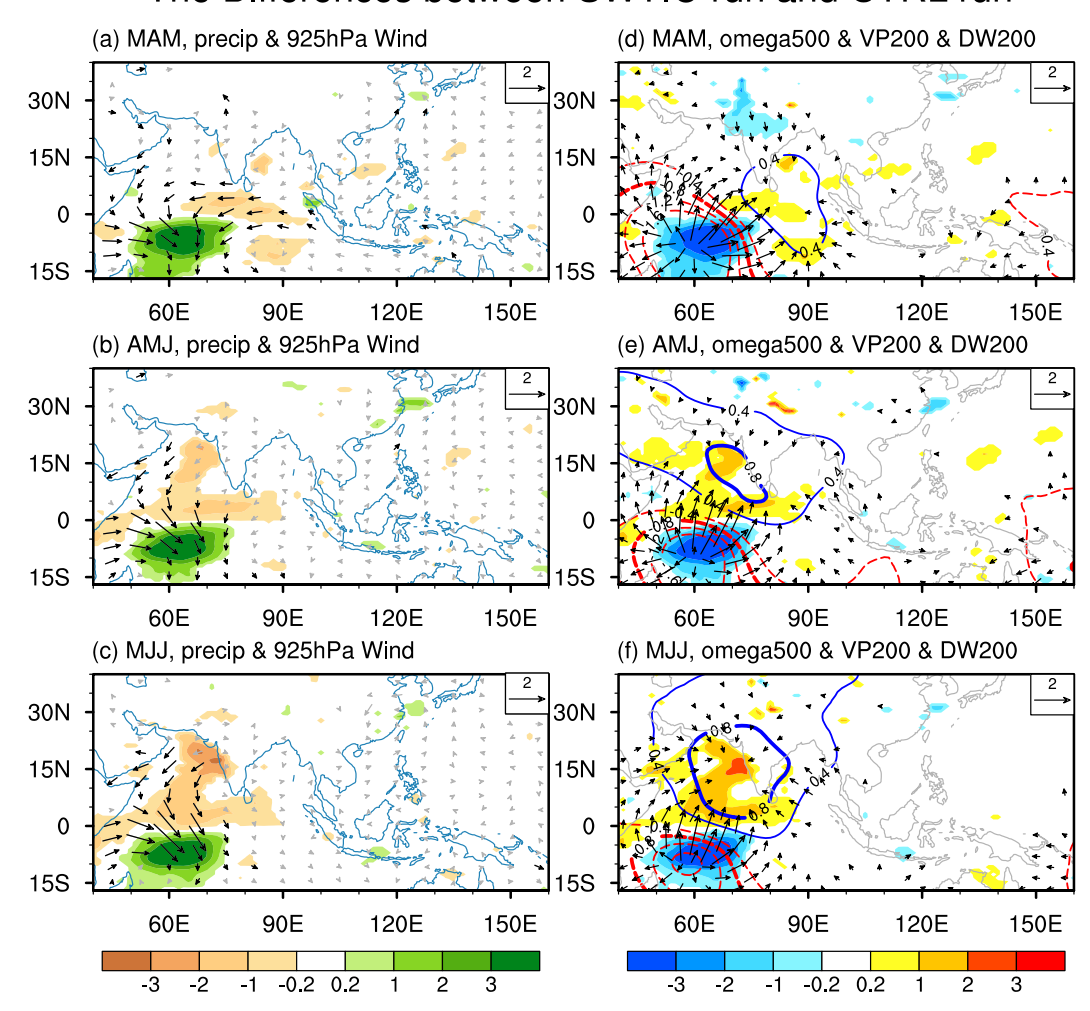


FIG. 10. As in Fig. 9, but for the differences between the SWTIO run and CTRL run.

In the SWTIO run, wind, precipitation, and velocity potential responses are similar to those in the SETIO run except that the entire pattern is located in the western TIO (Fig. 10). The observed asymmetric precipitation and wind anomaly pattern over the western TIO seems to be captured by the SWTIO run although the model response seems to be stronger than observations (Figs. 6 and 10). The southwest TIO warming appears to significantly affect the in situ and Arabian Sea climate. However, the signal over the eastern TIO is relatively weak in the SWTIO run. Besides, the simulated precipitation and atmospheric circulation in the South China Sea and its adjacent area in SWTIO run are weaker and less significant than those in the SETIO run (Figs. 8 and 10). The SWTIO run suggests that the southwest TIO SST anomalies only can directly influence the western TIO.

However, southwest TIO warming may indirectly exert its impact on the East Asian-western North Pacific climate (Xie et al. 2016). In fact, the southwest TIO warming could induce northwest Indian Ocean warming via the northeasterly wind response in the Arabian Sea when the southwest Asian monsoon prevails in the north Indian Ocean (Fig. 10). As the climatological lower troposphere winds over the north Indian Ocean turn into southwesterly in monsoon seasons, the north Indian Ocean warming peaks again due to the decreased southwesterly wind and reduced latent flux loss from the ocean. The western TIO warming may trigger atmospheric Kelvin wave propagating eastward into the Maritime Continent and western Pacific, sustaining the anticyclonic wind anomalies over western North Pacific (e.g., Xie et al. 2009, 2016). Such features can be clearly seen from the regression map with respect to the SWTIO SST index (Fig. 10).

## Cross Correlations between Two Variables

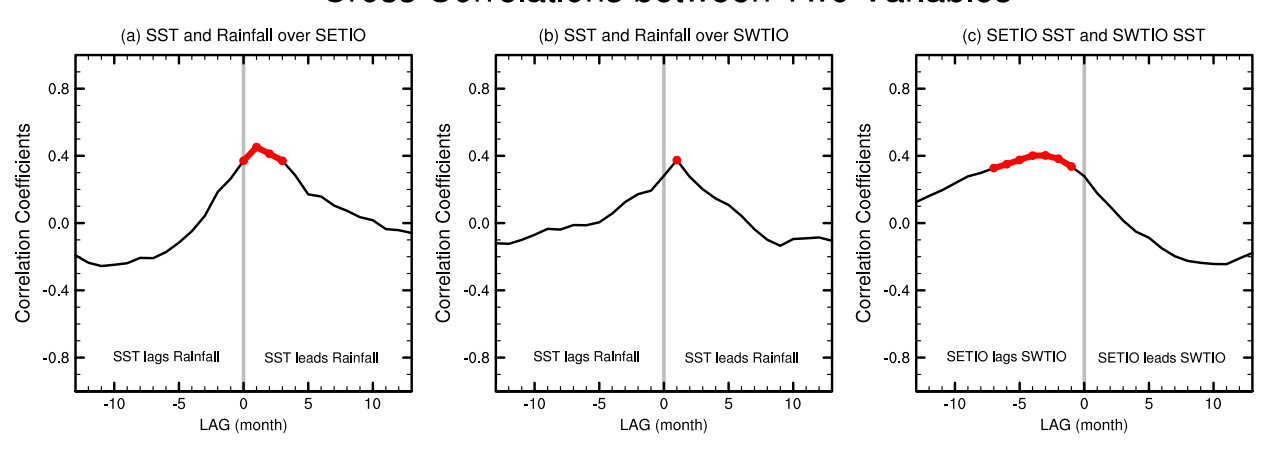


FIG. 11. Cross correlation between two monthly variables from 1979 to 2016: (a) southeast TIO SST and in situ rainfall, (b) southwest TIO SST and in situ rainfall, and (c) southeast TIO SST and southwest TIO SST. The range of the southeast (southwest) TIO is 12.5°–2.5°S, 90°–112.5°E (12.5°–2.5°S, 50°–80°E). The red dots signify that the correlation coefficients are significant at the 95% confidence level according to the two-tailed Student's *t* test.

# 5. The oceanic connection between southeast and southwest TIO warming

The south tropical Indian Ocean (TIO) warms during strong El Niño, exerting its influence on Indo-Pacific climate from spring to early summer. However, the southwest and southeast TIO warming seems not to be in the same pace. The lead–lag relationship between southeast and southwest TIO SST signifies that the southwest TIO warming (cooling) leads southeast TIO warming (cooling) by about 1 season (Fig. 11c). This lagged warming in the southeast TIO is expected because there is typically an anomalous cooling associated with a preceding positive Indian Ocean dipole (e.g., Tokinaga and Tanimoto 2004; Zhang and Yang 2007).

Figure 12 shows the composited sea surface height, sea surface wind, and SST anomalies for strong El Niño cases. The southwest TIO warming persists from boreal fall to ensuing early summer, while the southeast TIO warming begins in boreal winter and is sustained into summer (Fig. 12). From fall to winter, easterly wind anomalies prevail in the equatorial Indian Ocean with anticyclonic wind stress curls in the central to eastern part of south TIO (Fig. 12). Such changes facilitate the genesis of oceanic Rossby wave there (e.g., Xie et al. 2002). Anomalous positive sea surface height appears in the western to central part of the south TIO with its maximum intensity in boreal winter (Fig. 12). When the positive sea surface height anomalies over the southwest TIO gradually decay from D(-1)JF(0) to MJJ(0), positive sea surface height anomalies gradually develop near the Sumatra and Java Island. And the positive sea surface height anomalies feature an eastward movement

along the equator from D(-1)JF(0). Note that there are no strong westerly wind anomalies near the equator. Such eastward movement of sea surface height anomalies may be a result of eastward propagating Kelvin waves.

Using the AVISO daily output, we display the Hovmöller diagram for sea surface height along the south TIO and equator over strong El Niño cases. We can clearly see westward-propagating anomalous sea surface height along the south TIO (Fig. 13). They may dissipate along their westward journey (Fig. 13). However, when they reach the western boundary of south TIO (about 40°E), anomalous sea surface height quickly propagates eastward along the equator (Fig. 13). The reflected signatures form eastward-propagating oceanic Kelvin waves and quickly reach the Sumatra coast. The incoming oceanic Kelvin waves induce the southeast TIO warming via deepening the thermocline and suppressing the oceanic damping at the base of the mixed layer. Such oceanic processes provide an ocean dynamic explanation of why southeast TIO SST variation tends to lag the southwest TIO SST variation by about one season (Fig. 11c).

### 6. Summary and discussion

East Asian climate during early summer is significantly associated with SST variability in two subregions of the south TIO: the southwest TIO, which is also referred to as the thermocline dome (e.g., Xie et al. 2002) or Seychelles–Chagos thermocline ridge (Izumo et al. 2008), and the southeast TIO. In this study, we explore the influence of the south TIO on north Indian Ocean

## Sea Surface Height, Surface Wind and SST Anomalies

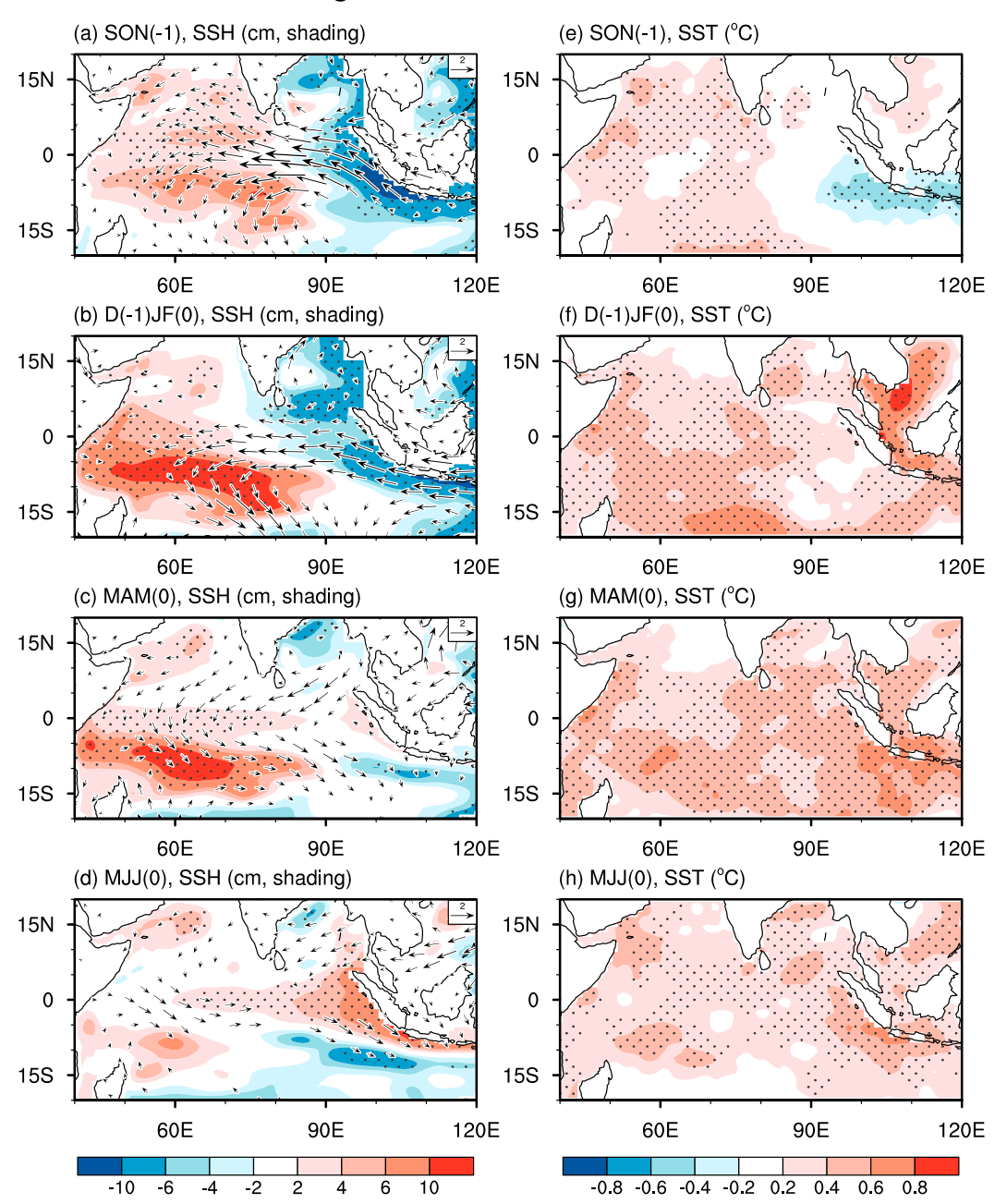


FIG. 12. Composited sea surface height (cm; shading) and surface wind and SST (°C) anomalies from the previous fall to the following summer for strong El Niño cases. Here, the numerals -1 and 0 denote the El Niño developing and decaying year, respectively. Stippling (black vectors) indicates the sea surface height and SST (surface wind) anomalies are significant at the 95% (90%) confidence level based on the two-tailed Student's t test.

and East Asian climate following a strong El Niño. Both the southwest and southeast TIO warming, which take place following a strong El Niño, modulate the Indo-Pacific climate during early summer.

The southwest TIO warming induces asymmetric wind anomalies over most of the TIO with anomalous

northeasterly winds north of the equator and anomalous northwesterly winds south of the equator. With the prevailing southwesterly winds over the north Indian Ocean, the northeasterly wind anomalies forced by southwest TIO warming decrease surface wind speed and latent heat flux, helping warm much of the north

## Sea Surface Height Anomalies

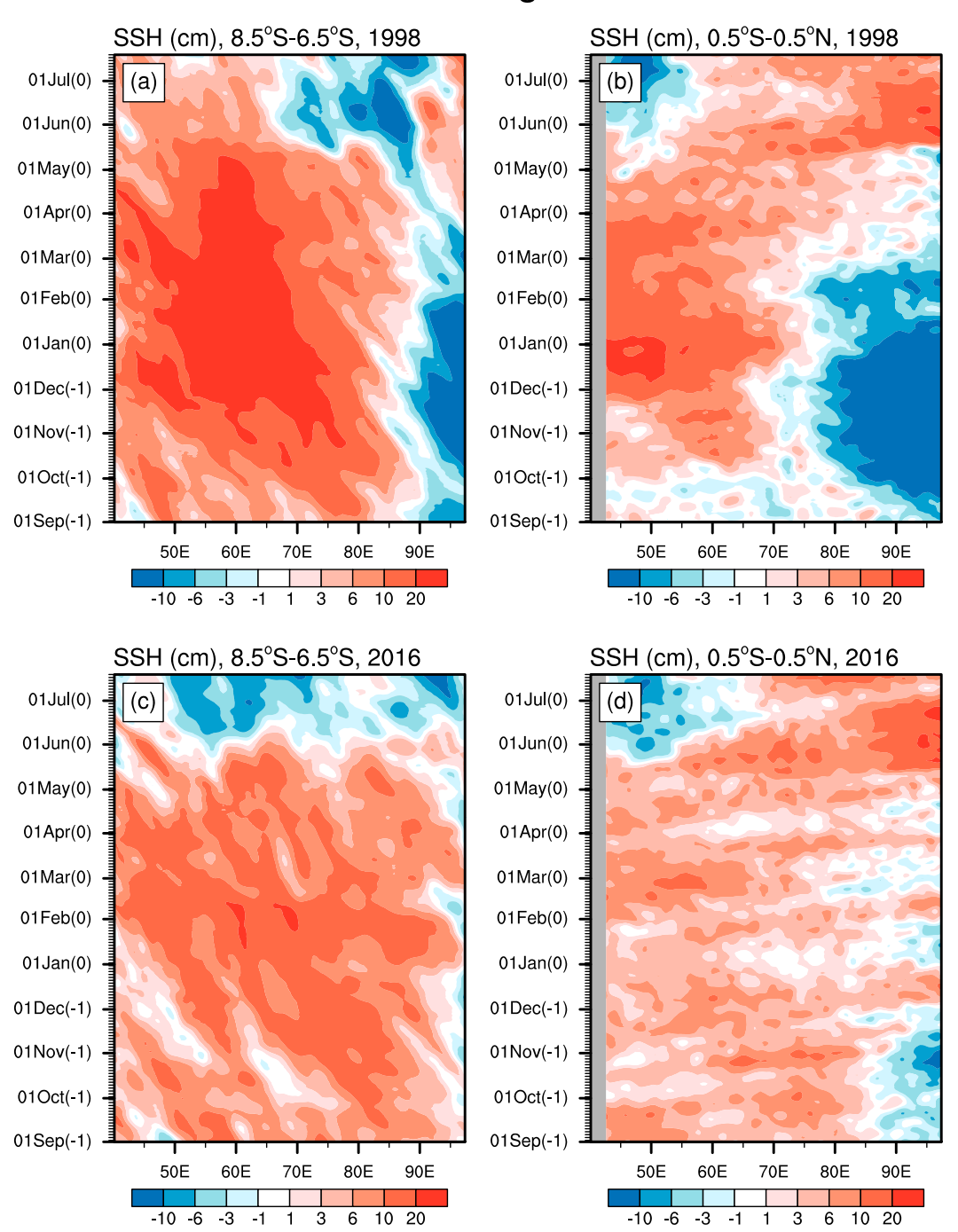


FIG. 13. The evolution of sea surface height (cm) anomalies along (a),(c) the south tropical Indian Ocean (average between  $8.5^{\circ}$  and  $6.5^{\circ}$ S) and (b),(d) the equator (average between  $0.5^{\circ}$ S and  $0.5^{\circ}$ N) from September (-1) to July (0) for strong El Niño cases. Here, the numerals -1 and 0 denote the El Niño developing and decaying year, respectively.

Indian Ocean. The TIO warming during early summer affects East Asia through a Kelvin wave-induced Ekman divergence mechanism (Xie et al. 2009).

The springtime southwest TIO warming is related to the El Niño condition in the previous winter. Ocean dynamics and oceanic Rossby waves are crucial for maintaining the southwest TIO warming. Downwelling oceanic Rossby waves associated with El Niño slowly propagate westward, which deepen the thermocline and contribute to SST warming in the SWTIO where the mean thermocline is shallow (e.g., Xie et al. 2002; Du et al. 2009). We also found that the springtime southeast TIO SST is significantly correlated with previous wintertime ENSO. The eastward propagating oceanic Kelvin waves, coming from the reflection of slowly propagating downwelling oceanic Rossby waves, seem to be conducive to southeast TIO warming. The oceanic Kelvin waves help maintain the southeast TIO warming via deepening the thermocline and suppressing the coastal upwelling induced by cross-equatorial winds in monsoon seasons. Such ocean dynamic processes can partly explain the lag relationship between the southwest and southeast TIO warming. A strong southeast TIO warming during boreal spring or early summer happens only following a strong, especially extreme, El Niño. In the observational record, the extreme El Niño is rare and each seems to have different characteristics. As a result, the role of southeast TIO warming in post-El Niño years in modulating East Asian climate has not been fully investigated in previous studies.

Our work reveals that the southeast TIO warming also anchors a "C-shaped" wind anomaly pattern over the eastern Indian Ocean, as the SWTIO warming does in the western TIO. The anomalous easterly wind response to southeast TIO warming in turn helps sustain the warming in the Bay of Bengal and South China Sea after the onset of the southwest monsoon. Besides, the southeast TIO warming induces a local meridional circulation with the ascending (descending) branch over the southeast (northeast) TIO. The anomalous downdraft over the South China Sea and the Philippines in turn helps maintain the anomalous anticyclonic circulation over the western North Pacific. In fact, while both the southwest and southeast TIO warming induce a similar cross-equatorial circulation pattern, the southeast TIO warming is far more influential on the rainfall and surface wind response over the Bay of Bengal and South China Sea (Figs. 9 and 10) by virtue of closer geographic proximity.

It is reported that the anticyclonic circulation response over the western North Pacific to symmetric TIO basin warming is too weak in the AGCM experiment (e.g., Xie et al. 2009). One plausible explanation is that

the AGCM lacks air-sea interaction. As a result, the simulated monsoon rainfall is weaker than observations (Kang et al. 2002), limiting the convection-circulation feedback over the subtropical Pacific, and thus the simulated atmospheric response to symmetric TIO warming cannot reach the observed magnitude (Xie et al. 2009). In fact, the observed low-level circulation and precipitation anomalies over the tropical western Pacific are rather asymmetric, more pronounced north than south of the equator (Figs. 6 and 7). Such asymmetric features over the tropical western Pacific can result from strong Asian summer monsoon rainfall in the mean state and thus the strong convection-circulation feedback (Xie et al. 2009). Another plausible reason is the lack of cold SST anomalies in the North Pacific that coexist with TIO SST warming in observations and influence circulation to the west via a Rossby wave-type response (Wu et al. 2014). However, we argue that the forcing of southeast TIO SST anomalies may also play a role in shaping such asymmetric feature by inducing local meridional circulation anomalies.

Acknowledgments. We thank three anonymous reviewers for their comments and suggestions that help improve the manuscript. This work is jointly supported the National Natural Science Foundation of China (41830538, 41805057, 41525019, 41775085), the State Oceanic Administration of China (GASIIPOV AI-02), and the Guangdong Natural Science Foundation (2018A030310023). The authors gratefully acknowledge the use of the High-Performance Computing Center (HPCC) at the South China Sea Institute of Oceanology, Chinese Academy of Sciences. The authors declare that they have no conflict of interest.

### REFERENCES

Adler, R. F., and Coauthors, 2003: The version-2 Global Precipitation Climatology Project (GPCP) monthly precipitation analysis (1979–present). J. Hydrometeor., 4, 1147–1167, https://doi.org/ 10.1175/1525-7541(2003)004<1147:TVGPCP>2.0.CO;2.

An, S.-I., and B. Wang, 2001: Mechanisms of locking the El Niño and La Niña mature phases to boreal winter. J. Climate, 14, 2164–2176, https://doi.org/10.1175/1520-0442(2001)014<2164: MOLOTE>2.0.CO:2.

Annamalai, H., P. Liu, and S.-P. Xie, 2005: Southwest Indian Ocean SST variability: Its local effect and remote influence on Asian monsoons. *J. Climate*, **18**, 4150–4167, https://doi.org/10.1175/JCLI3533.1.

Chen, J., Z. Wen, R. Wu, Z. Chen, and P. Zhao, 2014: Interdecadal changes in the relationship between southern China winterspring precipitation and ENSO. *Climate Dyn.*, 43, 1327–1338, https://doi.org/10.1007/s00382-013-1947-x.

Chen, W., 2002: Impacts of El Niño and La Niña on the cycle of the East Asian winter and summer monsoon (in Chinese). *Chin. J. Atmos. Sci.*, 26, 595–610.

- Chen, Z., Z. Wen, R. Wu, X. Lin, and J. Wang, 2016: Relative importance of tropical SST anomalies in maintaining the western North Pacific anomalous anticyclone during El Niño to La Niña transition years. *Climate Dyn.*, 46, 1027–1041, https://doi.org/10.1007/s00382-015-2630-1.
- —, —, and Y. Du, 2017: Roles of tropical SST anomalies in modulating the western north Pacific anomalous cyclone during strong La Niña decaying years. *Climate Dyn.*, **49**, 633– 647, https://doi.org/10.1007/s00382-016-3364-4.
- ——, Y. Du, Z. Wen, R. Wu, and C. Wang, 2018: Indo-Pacific climate during the decaying phase of the 2015/16 El Niño: Role of southeast tropical Indian Ocean warming. *Climate Dyn.*, 50, 4707–4719, https://doi.org/10.1007/s00382-017-3899-z.
- Dee, D. P., and Coauthors, 2011: The ERA-Interim reanalysis: Configuration and performance of the data assimilation system. *Quart. J. Roy. Meteor. Soc.*, 137, 553–597, https://doi.org/10.1002/qj.828.
- Du, Y., S.-P. Xie, G. Huang, and K. Hu, 2009: Role of air–sea interaction in the long persistence of El Niño–induced north Indian Ocean warming. *J. Climate*, 22, 2023–2038, https://doi.org/10.1175/2008JCLI2590.1.
- ——, L. Yang, and S.-P. Xie, 2011: Tropical Indian Ocean influence on northwest Pacific tropical cyclones in summer following strong El Niño. J. Climate, 24, 315–322, https://doi.org/10.1175/ 2010JCLI3890.1.
- Galanti, E., and E. Tziperman, 2000: ENSO's phase locking to the seasonal cycle in the fast-SST, fast-wave, and mixed-mode regimes. J. Atmos. Sci., 57, 2936–2950, https://doi.org/10.1175/ 1520-0469(2000)057<2936:ESPLTT>2.0.CO;2.
- Gent, P. R., and Coauthors, 2011: The Community Climate System Model version 4. J. Climate, 24, 4973–4991, https://doi.org/ 10.1175/2011JCLI4083.1.
- He, Z., and R. Wu, 2014: Indo-Pacific remote forcing in summer rainfall variability over the South China Sea. *Climate Dyn.*, 42, 2323–2337, https://doi.org/10.1007/s00382-014-2123-7.
- ——, and W. Wang, 2016: Signals of the South China Sea summer rainfall variability in the Indian Ocean. *Climate Dyn.*, **46**, 3181–3195, https://doi.org/10.1007/s00382-015-2760-5.
- Hu, K., G. Huang, and R. Huang, 2011: The impact of tropical Indian Ocean variability on summer surface air temperature in China. J. Climate, 24, 5365–5377, https://doi.org/10.1175/2011JCLI4152.1.
- —, —, X.-T. Zheng, S.-P. Xie, X. Qu, Y. Du, and L. Liu, 2014: Interdecadal variations in ENSO influences on northwest Pacific–East Asian early summertime climate simulated in CMIP5 models. J. Climate, 27, 5982–5998, https://doi.org/ 10.1175/JCLI-D-13-00268.1.
- Hu, W., R. Wu, and Y. Liu, 2014: Relation of the South China Sea precipitation variability to tropical Indo-Pacific SST anomalies during spring-to-summer transition. *J. Climate*, 27, 5451– 5467, https://doi.org/10.1175/JCLI-D-14-00089.1.
- Huang, B., and J. L. Kinter, 2002: Interannual variability in the tropical Indian Ocean. J. Geophys. Res., 107, 3199, https:// doi.org/10.1029/2001JC001278.
- Hurrell, J., J. Hack, D. Shea, J. Caron, and J. Rosinski, 2008: A new sea surface temperature and sea ice boundary dataset for the Community Atmosphere Model. J. Climate, 21, 5145–5153, https://doi.org/10.1175/2008JCLI2292.1.
- Izumo, T., C. de Boyer Montégut, J.-J. Luo, S. K. Behera, S. Masson, and T. Yamagata, 2008: The role of the western Arabian Sea upwelling in Indian monsoon rainfall variability. *J. Climate*, 21, 5603–5623, https://doi.org/10.1175/2008JCLJ2158.1.
- Kang, I.-S., and Coauthors, 2002: Intercomparison of the climatological variations of Asian summer monsoon precipitation

- simulated by 10 GCMs. *Climate Dyn.*, **19**, 383–395, https://doi.org/10.1007/s00382-002-0245-9.
- Klein, S. A., B. J. Soden, and N.-C. Lau, 1999: Remote sea surface temperature variations during ENSO: Evidence for a tropical atmospheric bridge. *J. Climate*, 12, 917–932, https://doi.org/ 10.1175/1520-0442(1999)012<0917:RSSTVD>2.0.CO:2.
- Kosaka, Y., S.-P. Xie, N.-C. Lau, and G. A. Vecchi, 2013: Origin of seasonal predictability for summer climate over the northwestern Pacific. *Proc. Natl. Acad. Sci. USA*, 110, 7574–7579, https://doi.org/10.1073/pnas.1215582110.
- Kug, J.-S., T. Li, S.-I. An, I.-S. Kang, J.-J. Luo, S. Masson, and T. Yamagata, 2006: Role of the ENSO-Indian Ocean coupling on ENSO variability in a coupled GCM. *Geophys. Res. Lett.*, 33, L09710, https://doi.org/10.1029/2005GL024916.
- Lin, S., 2004: A "vertically Lagrangian" finite-volume dynamical core for global models. *Mon. Wea. Rev.*, **132**, 2293–2307, https:// doi.org/10.1175/1520-0493(2004)132<2293:AVLFDC>2.0.CO;2.
- Liu, Z., and M. Alexander, 2007: Atmospheric bridge, oceanic tunnel, and global climatic teleconnections. *Rev. Geophys.*, 45, RG2005, https://doi.org/10.1029/2005RG000172.
- Moron, V., A. Lucero, F. Hilario, B. Lyon, A. W. Robertson, and D. DeWitt, 2009: Spatio-temporal variability and predictability of summer monsoon onset over the Philippines. *Climate Dyn.*, 33, 1159–1177, https://doi.org/10.1007/s00382-008-0520-5.
- Neale, R. B., J. Richter, S. Park, P. H. Lauritzen, S. J. Vavrus, P. J. Rasch, and M. Zhang, 2013: The mean climate of the Community Atmosphere Model (CAM4) in forced SST and fully coupled experiments. *J. Climate*, 26, 5150–5168, https://doi.org/10.1175/JCLI-D-12-00236.1.
- Nguyen-Le, D., J. Matsumoto, and T. Ngo-Duc, 2015: Onset of the rainy seasons in the eastern Indochina Peninsula. *J. Climate*, **28**, 5645–5666, https://doi.org/10.1175/JCLI-D-14-00373.1.
- North, G. R., T. L. Bell, R. F. Cahalan, and F. J. Moeng, 1982: Sampling errors in the estimation of empirical orthogonal functions. *Mon. Wea. Rev.*, **110**, 699–706, https://doi.org/10.1175/1520-0493(1982)110<0699:SEITEO>2.0.CO;2.
- Okumura, Y. M., and C. Deser, 2010: Asymmetry in the duration of El Niño and La Niña. *J. Climate*, **23**, 5826–5843, https://doi.org/10.1175/2010JCLI3592.1.
- Qu, X., and G. Huang, 2012: Impacts of tropical Indian Ocean SST on the meridional displacement of East Asian jet in boreal summer. Int. J. Climatol., 32, 2073–2080, https://doi.org/10.1002/joc.2378.
- Rasmusson, E. M., and T. H. Carpenter, 1982: Variations in tropical sea surface temperature and surface wind fields associated with the Southern Oscillation/El Niño. *Mon. Wea. Rev.*, **110**, 354–384, https://doi.org/10.1175/1520-0493(1982)110<0354: VITSST>2.0.CO;2.
- Rayner, N. A., D. E. Parker E. B. Horton C. K. Folland L. V. Alexander D. P. Rowell E. C. Kent A. Kaplan, 2003: Global analyses of sea surface temperature, sea ice, and night marine air temperature since the late nineteenth century. *J. Geophys. Res.*, 108, 4407, https://doi.org/10.1029/2002JD002670.
- Taylor, K., D. Williamson, and F. Zwiers, 2000: The sea surface temperature and sea-ice concentration boundary conditions for AMIP II simulations. PCMDI Rep. 60, 28 pp., https:// pcmdi.llnl.gov/report/ab60.html.
- Tokinaga, H., and Y. Tanimoto, 2004: Seasonal transition of SST anomalies in the tropical Indian Ocean during El Niño and IOD years. *J. Meteor. Soc. Japan*, **82**, 1007–1018, https://doi.org/10.2151/jmsj.2004.1007.
- Tziperman, E., S. E. Zebiak, and M. A. Cane, 1997: Mechanisms of seasonal–ENSO interaction. *J. Atmos. Sci.*, **54**, 61–71, https://doi.org/10.1175/1520-0469(1997)054<0061:MOSEI>2.0.CO;2.

- Wang, B., R. Wu, and X. Fu, 2000: Pacific–East Asian teleconnection: How does ENSO affect East Asian climate? *J. Climate*, 13, 1517–1536, https://doi.org/10.1175/1520-0442(2000) 013<1517:PEATHD>2.0.CO;2.
- —, and T. Li, 2003: Atmosphere–warm ocean interaction and its impacts on Asian-Australian monsoon variation. *J. Climate*, **16**, 1195–1211, https://doi.org/10.1175/1520-0442(2003) 16<1195:AOIAII>2.0.CO;2.
- —, LinHo, Y. Zhang, and M.-M. Lu, 2004: Definition of South China Sea monsoon onset and commencement of the East Asia summer monsoon. *J. Climate*, **17**, 699–710, https://doi.org/10.1175/2932.1.
- Wang, C., R. H. Weisberg, J. Virmani, 1999: Western Pacific interannual variability associated with the El Niño-Southern Oscillation. J. Geophys. Res., 104, 5131–5149, https://doi.org/10.1029/1998JC900090.
- Watanabe, M., and F. Jin, 2002: Role of Indian Ocean warming in the development of Philippine Sea anticyclone during ENSO. Geophys. Res. Lett., 29, 1478, https://doi.org/10.1029/2001GL014318.
- Weisberg, R. H., and C. Wang, 1997: A western Pacific oscillator paradigm for the El Niño–Southern Oscillation. *Geophys. Res. Lett.*, 24, 779–782, https://doi.org/10.1029/97GL00689.
- Wu, B., T. Li, and T. Zhou, 2010: Relative contributions of the Indian Ocean and local SST anomalies to the maintenance of the western North Pacific anomalous anticyclone during the El Niño decaying summer. J. Climate, 23, 2974–2986, https:// doi.org/10.1175/2010JCLI3300.1.
- Wu, R., and S.-W. Yeh, 2010: A further study of the tropical Indian Ocean asymmetric mode in boreal spring. *J. Geophys. Res.*, **115**, D08101, https://doi.org/10.1029/2009JD012999.
- —, and W. Hu, 2015: Air–sea relationship associated with precipitation anomaly changes and mean precipitation anomaly over the South China Sea and the Arabian Sea during the spring to summer transition. *J. Climate*, 28, 7161–7181, https://doi.org/10.1175/JCLI-D-15-0136.1.
- —, Z.-Z. Hu, and B. P. Kirtman, 2003: Evolution of ENSOrelated rainfall anomalies in East Asia. *J. Climate*, **16**, 3742– 3758, https://doi.org/10.1175/1520-0442(2003)016<3742: EOERAI>2.0.CO;2.
- ——, B. P. Kirtman, and V. Krishnamurthy, 2008: An asymmetric mode of tropical Indian Ocean rainfall variability in boreal spring. *J. Geophys. Res.*, **113**, D05104, https://doi.org/10.1029/ 2007JD009316.
- —, S. Yang, Z. Wen, G. Huang, and K. Hu, 2012: Interdecadal change in the relationship of southern China summer rainfall with tropical Indo-Pacific SST. *Theor. Appl. Climatol.*, **108**, 119–133, https://doi.org/10.1007/s00704-011-0519-4.
- —, G. Huang, Z. Du, and K. Hu, 2014: Cross-season relation of the South China Sea precipitation variability between winter and summer. *Climate Dyn.*, 43, 193–207, https://doi.org/ 10.1007/s00382-013-1820-y.
- Wu, Y.-K., C.-C. Hong, and C.-T. Chen, 2018: Distinct effects of the two strong El Niño events in 2015–2016 and 1997–1998 on the western North Pacific monsoon and tropical cyclone ac-

- tivity: Role of subtropical eastern North Pacific warm SSTA. *J. Geophys. Res. Oceans*, **123**, 3603–3618, https://doi.org/10.1002/2018JC013798.
- Xie, S.-P., 1996: Westward propagation of latitudinally asymmetry in a coupled ocean–atmosphere model. *J. Atmos. Sci.*, **53**, 3236–3250, https://doi.org/10.1175/1520-0469(1996)053<3236: WPOLAI>2.0.CO;2.
- —, and S. G. H. Philander, 1994: A coupled ocean–atmosphere model of relevance to the ITCZ in the eastern Pacific. *Tellus*, 46A, 340–350, https://doi.org/10.3402/tellusa.v46i4.15484.
- ——, H. Annamalai, F. A. Schott, and J. P. McCreary, 2002: Structure and mechanisms of South Indian Ocean climate variability. J. Climate, 15, 864–878, https://doi.org/10.1175/ 1520-0442(2002)015<0864:SAMOSI>2.0.CO;2.
- —, K. Hu, J. Hafner, H. Tokinaga, Y. Du, G. Huang, and T. Sampe, 2009: Indian Ocean capacitor effect on Indowestern Pacific climate during the summer following El Niño. J. Climate, 22, 730–747, https://doi.org/10.1175/ 2008JCLI2544.1.
- —, Y. Kosaka, Y. Du, K. Hu, J. Chowdary, and G. Huang, 2016: Indo-western Pacific Ocean capacitor and coherent climate anomalies in post-ENSO summer: A review. *Adv. Atmos. Sci.*, **33**, 411–432, https://doi.org/10.1007/s00376-015-5192-6.
- Yang, J., Q. Liu, S.-P. Xie, Z. Liu, and L. Wu, 2007: Impact of the Indian Ocean SST basin mode on the Asian summer monsoon. *Geophys. Res. Lett.*, 34, L02708, https://doi.org/10.1029/ 2006GL028571.
- Yang, Y., S.-P. Xie, Y. Du, and H. Tokinaga, 2015: Interdecadal difference of interannual variability characteristics of South China Sea SSTs associated with ENSO. J. Climate, 28, 7145– 7160, https://doi.org/10.1175/JCLI-D-15-0057.1.
- Yuan, Y., W. Zhou, J. C.-L. Chan, and C. Li, 2008: Impacts of the basin-wide Indian Ocean SSTA on the South China Sea summer monsoon onset. *Int. J. Climatol.*, 28, 1579–1587, https://doi.org/10.1002/joc.1671.
- Zhan, R., Y. Wang, and X. Lei, 2011: Contributions of ENSO and east Indian Ocean SSTA to the interannual variability of northwest Pacific tropical cyclone frequency. *J. Climate*, **24**, 509–521, https://doi.org/10.1175/2010JCLI3808.1.
- Zhang, Q., and S. Yang, 2007: Seasonal phase-locking of peak events in the eastern Indian Ocean. *Adv. Atmos. Sci.*, **24**, 781–798, https://doi.org/10.1007/s00376-007-0781-7.
- Zhang, R., A. Sumi, and M. Kimoto, 1996: Impact of El Niño on the East Asian monsoon: A diagnostic study of the '86/87 and '91/92 events. *J. Meteor. Soc. Japan*, **74**, 49–62, https://doi.org/10.2151/jmsj1965.74.1\_49.
- —, —, and —, 1999: A diagnostic study of the impact of El Niño on the precipitation in China. *Adv. Atmos. Sci.*, **16**, 229–241, https://doi.org/10.1007/BF02973084.
- Zhou, Z.-Q., S.-P. Xie, G. J. Zhang, and W. Zhou, 2018: Evaluating AMIP skill in simulating interannual variability of summer rainfall over the Indo-western Pacific. *J. Climate*, **31**, 2253–2265, https://doi.org/10.1175/JCLI-D-17-0123.1.